



Ab initio study of adsorption and diffusion of lithium on transition metal dichalcogenide monolayers

Xiaoli Sun and Zhiguo Wang*

Full Research Paper

Open Access

Address:

School of Physical Electronics, University of Electronic Science and Technology of China, Chengdu, 610054, P.R. China

Email:

Zhiguo Wang* - zgwang@uestc.edu.cn

* Corresponding author

Keywords:

anode materials; lithium adsorption; lithium diffusion; lithium ion batteries; transition metal dichalcogenide

Beilstein J. Nanotechnol. **2017**, *8*, 2711–2718.

doi:10.3762/bjnano.8.270

Received: 02 July 2017

Accepted: 19 November 2017

Published: 15 December 2017

Associate Editor: P. Leiderer

© 2017 Sun and Wang; licensee Beilstein-Institut.

License and terms: see end of document.

Abstract

Using first principles calculations, we studied the stability and electronic properties of transition metal dichalcogenide monolayers of the type MX_2 ($\text{M} = \text{Ti, Zr, Hf, V, Nb, Ta, Mo, Cr, W}$; $\text{X} = \text{S, Se, Te}$). The adsorption and diffusion of lithium on the stable MX_2 phase was also investigated for potential application as an anode for lithium ion batteries. Some of these compounds were found to be stable in the 2H phase and some are in the 1T or 1T' phase, but only a few of them were stable in both 2H/1T or 2H/1T' phases. The results show that lithium is energetically favourable for adsorption on MX_2 monolayers, which can be semiconductors with a narrow bandgap and metallic materials. Lithium cannot be adsorbed onto 2H- WS_2 and 2H- WSe_2 , which have large bandgaps of 1.66 and 1.96 eV, respectively. The diffusion energy barrier is in the range between 0.17 and 0.64 eV for lithium on MX_2 monolayers, while for most of the materials it was found to be around 0.25 eV. Therefore, this work illustrated that most of the MX_2 monolayers explored in this work can be used as promising anode materials for lithium ion batteries.

Introduction

Lithium ion batteries (LIBs) have been widely used in portable electronic devices as power supplies, which have potential use in electrical vehicles (EVs) and smart grids. However, the energy and power density of current LIBs cannot satisfy the high demand of EVs. The development of new electrode materials is essential for improvement of the energy density. An ideal electrode material for LIBs should have good electronic conductivity, a lower Li diffusion energy barrier, as well as high energy and power densities. By reducing the bulk electrode materials to low-dimensional materials, a higher energy capacity

and higher charge/discharge rate can be obtained as the low-dimensional materials have higher exposure to the electrolyte [1]. Two-dimensional materials, such as Co_3O_4 , NiO, phosphorene, SnS and V_2O_5 all exhibit an excellent capacity retention, rate performance, lower energy barrier and long cycling life compared to their bulk counterparts used as electrode materials for LIBs [2–8].

Two-dimensional transition metal dichalcogenides, MX_2 (where M and X correspond to transition metal and chalcogen atoms,

respectively), have been synthesized using different strategies, such as exfoliation [9,10], physical vapour deposition [11] and chemical vapour deposition [12–14]. MX_2 has received tremendous attention as an alternative to graphite for the anode material in LIBs [15,16]. In particular, MoS_2 has been well-investigated as an anode material for LIBs both theoretically and experimentally. A graphene like- MoS_2 /graphene composite was shown to exhibit a high specific capacity of 1400 mA h/g and good rate performance as well as cycling ability [17]. It was reported that MoS_2 zigzag nanoribbons are promising electrode materials for LIBs with a high power density and fast charge/discharge rates [18]. The presence of structural defects can enhance the adsorption of Li atoms onto two-dimensional materials. Different from the situation where Li atoms are trapped by the defects in graphene, the presence of structural defects does not affect the diffusion of lithium [19]. The main drawback of MoS_2 is its poor electrical conductivity. Various strategies have been developed to improve the electrochemical properties of MoS_2 as an anode for LIBs. Three-dimensional hierarchical structures constructed by assembling two-dimensional MoS_2 nanosheets can deliver a capacity of 1009 mAh/g at 500 mA/g after 500 cycles [20]. The formation of composites of MoS_2 with other materials, such as carbon-based materials and non-carbonaceous materials, can enhance the electromechanical properties of MoS_2 . Wang et al. [21] utilized a beneficial "bridging effect" of sulfur atoms to bind few-layered MoS_2 with graphene, which provided fast electron conductivity and excellent cycling stability and superior rate performance. The composites exhibited a high discharge capacity of 1546 mAh/g after 300 cycles. The MoS_2 composites grown on TiO_2 nanotubes show better rate capability with a reversible capacity of 461 mAh/g at 1000 mA/g, compared with the capacity of pure MoS_2 (129 mAh/g) at the same current density [22].

MX_2 monolayers have three types of crystalline structures, hexagonal structure (2H), octahedral structure (1T) and distorted

octahedral structure (1T') [23–25]. The structures depend on the arrangements of the M and X atoms. Phase transformation between the different phases occurs during the synthesis process and lithium/sodium intercalation [26–28]. Sun et al. [29] have studied the effect of electron doping on the stability of 2H- and 1T'- MoS_2 , and showed that electron doping can stabilize the crystal structure of 1T'- MoS_2 . The crystalline structure can also affect the energy conversion efficiency, for example in the hydrogen evolution reaction (HER). The basal plane of 2H- MoS_2 is inert [30], whereas that of 1T'- MoS_2 is catalytically active for HER [31]. Until now, there is no systematic study on the family of transition metal dichalcogenide monolayers used as anode for LIBs.

In this work, we studied the stability of MX_2 monolayers, and the adsorption and diffusion of Li on the stable MX_2 monolayers ($\text{M} = \text{Ti, Zr, Hf, V, Nb, Ta, Mo, Cr, W}$; $\text{X} = \text{S, Se, Te}$). These results are helpful for the design of two-dimensional transition metal dichalcogenide based electrodes for LIBs.

Results and Discussion

We systematically investigated the phase stability, Li adsorption and diffusion on MX_2 monolayers ($\text{M} = \text{Ti, Zr, Hf, V, Nb, Ta, Cr, Mo, W}$; $\text{X} = \text{S, Se, Te}$). The combination of these elements have twenty seven possible binary compound materials. Three phases, including 2H, 1T and 1T' structures, were all considered for each of the binary monolayers. All the three structures can be viewed as a positively charged, two-dimensional M atoms, lattice-sandwiched by two hexagonal lattices of negatively charged X atoms. Each M atom is surrounded by six nearest X atoms, and each X atom is connected to three nearest M atoms with ionic M–X bonds. The side and cross-views of the ball and stick models of the MX_2 monolayer are shown in Figure 1. The M atoms are located at the lattice positions of a hexagonal close-packed structure with a trigonal symmetry in the 2H- MX_2 phase (Figure 1a), whereas M atoms are located at

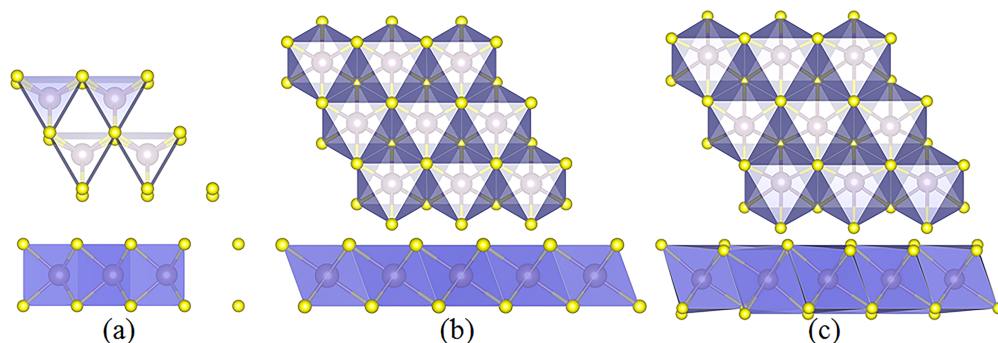


Figure 1: Top and side views of ball and stick models of a MX_2 monolayer in (a) 2H, (b) 1T and (c) 1T' phase. The M atoms have octahedral and trigonal prismatic coordination in the 1T/1T' and 2H phase, respectively.

the octahedral/disordered octahedral centre of six S atoms in the 1T/1T' phase (Figure 1b,c). Some compounds are not stable in the 1T' phase, which will be relaxed to the 1T phase after relaxation.

The energy related to the 2H phase per formula unit (f.u.), $E = E_{1T/1T'} - E_{2H}$, is listed in Table 1. A negative value indicates that the 1T/1T' phase is more stable than the 2H phase. It can be seen from the table that some of these compound can be stable in the 2H phase, and some in the 1T or 1T' phase. Only a few of them are stable both in 2H/1T or 2H/1T' phases. The 2H phase is the minimum energy configuration for monolayers of NbX₂ and TaX₂, which agrees with previously reported results [32,33]. The energy of the 1T phase is smaller than the 2H phase for TiX₂, VX₂, VSe₂, CrX₂, ZrX₂ and HfX₂. 1T-VS₂ monolayers are 0.02 eV/f.u. larger than the 2H phase, which indicates that the 1T phase is the energetically favourable one for these compounds, and VS₂ monolayers maybe be stable both in the 2H/1T phase. The results agree with other calculations that imply that the 1T phase is more stable than 2H in TiX₂ [32–34], CrS₂ [35], ZrX₂ [32,33] and HfX₂ [33]. The 2H phase is the stable structure for MoS₂, MoSe₂, WS₂ and WSe₂ monolayers, which has also been predicted by other simulations [36–40]. 1T'-VTe₂, 1T'-MoTe₂ and 1T'-WTe₂ are the energetically favourable phases. It is also can be seen from Table 1 that 1T'-MoTe₂ is 0.06 eV/f.u. more energetically favourable than the 1T phase, which agrees with other simulations [36,39,40]. The energy difference between 2H-WTe₂ and 1T'-WTe₂ is 0.07 eV/f.u., which indicates MoTe₂ and WTe₂ maybe exist in two phases.

The calculated lattice constants and bond length of the M–X bond in the stable phase is listed in Table 2 along with available values from other simulations. The values obtained in the present work agree well with other simulation results. It can be seen from Table 2 that lattice constants and bond lengths increase for the all the MX₂ monolayers as the element X

changes from S to Te in group VI for a given element M. The variation can be explained by the increasing atomic radius of elements X from S to Te.

The band structures of MX₂ monolayers in the stable phase are shown in Figure 2. The MX₂ monolayers can be semiconducting with a direct and indirect bandgap or metallic materials. The electronic conductive behaviour of these compounds are shown in Table 2. The 2H phase shows a semiconducting behaviour, such as 2H-WX₂, 2H-NbX₂, 2H-TaX₂ and 2H-MoX₂. The 1T phase can be metallic or semiconducting, such as in 1T-VX₂ (X = S, Se), and 1T-CrX₂ shows metallic behaviour, while 1T-TiX₂, 1T-ZrX₂ and 1T-HfX₂ show semiconducting and metallic behaviour with X = S/Se and X = Te, respectively. 1T'-VTe₂ and 1T'-MoTe₂ show metallic behaviour and 1T'-WTe₂ has a narrow bandgap of 0.50 eV. The obtained bandgap values are close to those previously reported for TiS₂ [32], CrTe₂ [40], TiX₂ [32,33,47], MoX₂ [33,40,47,50–55], HfX₂ [33,47] and WX₂ [33,40,47,50,55–58]. The metallic MX₂ monolayers have good electrical conductivity, which may make them good anode materials.

As shown in Figure 3a and Figure 3b, there are two stable adsorption sites, that is, the hollow site (H) and the top position above the M atom (T) for Li to be adsorbed on the 2H- and 1T-MX₂ monolayers [18]. Four adsorption sites (T1, T2, H1, and H2) are considered for Li adsorption onto the 1T'-MX₂ monolayer, as shown in Figure 3c. To analyse the stability of Li adsorbed on the MX₂ monolayers, the adsorption energy, $E_{ad}(Li)$, is calculated using Equation 1:

$$E_{ad}(Li) = E_{MX_2+Li} - E_{MX_2} - E_{Li}, \quad (1)$$

where E_{MX_2+Li} and E_{MX_2} are the total energy of the MX₂ monolayer with and without Li adsorption, respectively. E_{Li} is the energy of a Li atom in bulk material. The calculated adsorp-

Table 1: Energy (eV) referenced to the 2H phase per formula unit. A negative value indicates that the 1T/1T' phase is more stable than the 2H phase.

M	S			Se			Te		
	2H	1T	1T'	2H	1T	1T'	2H	1T	1T'
Ti	0.00	−0.44	–	0.00	−0.33	–	0.00	−0.26	–
V	0.00	0.02	–	0.00	−0.16	–	0.00	−0.06	−0.15
Cr	0.00	−0.45	–	0.00	−0.39	–	0.00	−0.17	–
Zr	0.00	−0.54	–	0.00	−0.40	–	0.00	−0.26	–
Nb	0.00	0.21	–	0.00	0.22	–	0.00	0.15	0.10
Mo	0.00	0.68	0.60	0.00	0.35	0.29	0.00	−0.20	−0.26
Hf	0.00	−0.62	–	0.00	−0.50	–	0.00	−0.35	–
Ta	0.00	0.18	–	0.00	0.23	0.21	0.00	0.15	0.54
W	0.00	0.91	0.61	0.00	0.81	0.35	0.00	0.61	−0.07

Table 2: Lattice constants (a, b) and the bond length of the M–X bond (d_{M-X}) in the stable phase as calculated in this work as compared to other values found in the literature from other simulations. The electronic conducting behaviour (ECB) of these compounds is also shown.

MX_2	a/b (Å)	d_{M-X} (Å)	a (Å) [Ref.]	d_{M-X} (Å) [Ref.]	ECB
1T-TiS ₂	3.40	2.42	3.39 [33]	2.39 [41]	0.59
1T-TiSe ₂	3.56	2.57	3.53 [33]	2.51 [41]	0.29
1T-TiTe ₂	3.72	2.77	3.74 [33]	2.73 [41]	metal
2H-VS ₂	3.19	2.39	3.17 [42-44]	2.36 [42-44]	0.58
1T-VS ₂	3.25	2.38	3.18 [43,45]	2.35 [43,44,46]	metal
1T-VSe ₂	3.37	2.55	3.24 [41]	2.49 [46]	metal
1T'-VTe ₂	3.80/ 7.60	2.71/ 2.76/ 2.79/ 2.81	–	–	metal
1T-CrS ₂	3.33	2.41	–	–	metal
1T-CrSe ₂	3.47	2.56	–	–	metal
1T-CrTe ₂	3.67	2.81	–	–	metal
1T-ZrS ₂	3.57	2.55	3.68 [33,47]		0.92
1T-ZrSe ₂	3.70	2.68	3.79 [47]		0.29
1T-ZrTe ₂	3.89	2.90	3.98 [33]		metal
2H-NbS ₂	3.35	2.50	3.36 [48]	2.49 [48]	1.22
2H-NbSe ₂	3.49	2.64	3.48 [48]	2.62 [48]	1.00
2H-NbTe ₂	3.71	2.83	3.70 [48]	2.82 [48]	0.78
2H-MoS ₂	3.17	2.42	3.18 [47,49]	2.42 [48]	1.71
2H-MoSe ₂	3.32	2.55	3.32 [47]	2.55 [48]	1.41
1T-MoTe ₂	3.84	2.81	–	–	metal
1T'-MoTe ₂	3.89/ 7.88	2.53/ 2.55/ 2.60/ 2.61	–	–	0.12
1T-HfS ₂	3.57	2.54	3.64 [33]	–	1.09
1T-HfSe ₂	3.69	2.67	3.76 [33]	–	0.50
1T-HfTe ₂	3.88	2.87	3.97 [33]	–	metal
2H-TaS ₂	3.35	2.50	3.34 [48]	2.48 [48]	0.20
2H-TaSe ₂	3.47	2.63	3.48 [48]	2.62 [48]	0.46
2H-TaTe ₂	3.69	2.82	3.76 [48]	2.82 [48]	0.37
2H-WS ₂	3.18	2.44	3.18 [49]	2.42 [48]	1.96
2H-WSe ₂	3.32	2.57	3.32 [47,48]	2.55 [48]	1.66
2H-WTe ₂	3.56	2.76	–	–	1.22
1T'-WTe ₂	3.49/ 6.98	2.74/ 2.75/ 2.78/ 2.81	–	–	0.38

tion energy of Li on the stable phase of the MX_2 monolayers is shown in Figure 4. The adsorption energy has positive values for Li adsorbed on 2H-WS₂ and 2H-WSe₂, which indicates that Li cannot be adsorbed on these two compounds and they are not ideal anodes for LIBs. The other compounds have negative values of adsorption energy. The adsorption energy of Li on 2H-MoS₂ is -0.05 and -0.25 eV for H and T sites, respectively. The materials will have a large energy storage capacity if they have a large exothermic reaction energy with Li [19]. Previous studies have shown that the 2H-MoS₂ monolayer is a good anode material for LIBs [26-28]. The absolute value of the

adsorption energy for Li adsorbed on other compounds is larger than that of 2H-MoS₂, so other MX_2 compounds are also good anode candidates for LIBs. The adsorption energy as a function of the bandgap of the MX_2 monolayer is shown in Figure 4. It can also be seen from the figure that MX_2 is a semiconducting material with a narrow bandgap, and for metallic materials, the adsorption energy has larger negative values. The materials with a large bandgap have smaller adsorption energy, even those with positive values. For example, the bandgap energies are 1.96, 1.71, 0.78, 0.58 and 0.29 eV and the adsorption energies for Li adsorbed at H/T sites are 0.37/0.24, $-0.05/-0.25$,

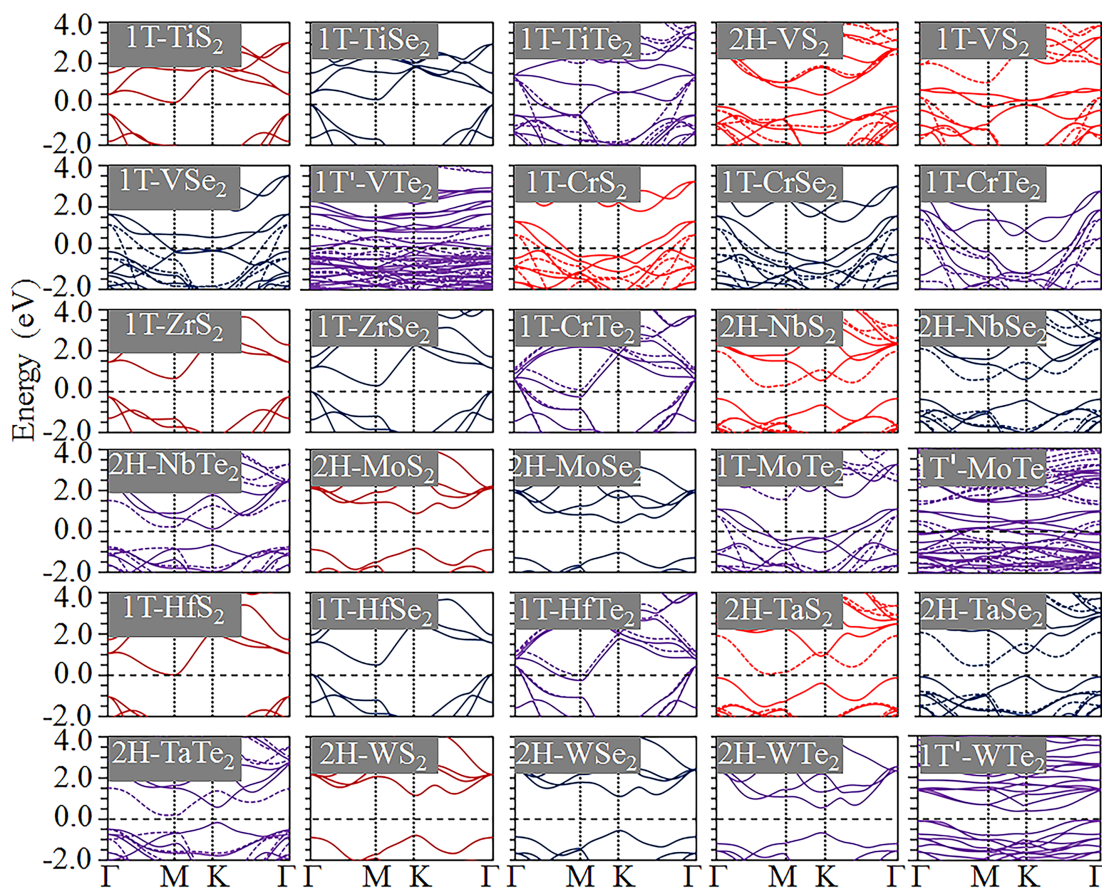


Figure 2: Band structures of MX₂ monolayers in the stable phase. Fermi energy level is set to be 0.

−0.51/−0.65, −1.79/1.87 and −2.08/2.07 eV on 2H-WS₂, 2H-MoS₂, 2H-NbTe₂, 2H-VS₂ and 1T-TiSe₂ monolayers, respectively.

The diffusion of Li on the MX₂ monolayers is through the T→H→T and T1→H1→T2→H2→T1 paths for the 2H/1T and 1T' phases, respectively [59], as shown in Figure 3a–c. The typical diffusion energy profiles are shown in Figure 3d, Figure 3e and Figure 3f for Li on 2H-MoS₂, 1T-TiS₂, and 1T'-MoTe₂ monolayers, respectively. The constrained method was used to evaluate the diffusion behaviour of Li on MX₂ monolayers – this method is more simple and intuitive compared to the nudged elastic band method and dimer method [60]. The diffusion energy barriers are 0.29, 0.25 and 0.28 eV for Li on 2H-MoS₂, 1T-TiS₂, and 1T'-MoTe₂ monolayers, respectively. These values are reasonable for use as anodes for LIBs. The Li diffusion energy barrier on a MX₂ monolayer is shown in Figure 4. Our calculated values agree well with those reported by other researchers. The diffusion energy barrier for Li on the 2H phase of monolayer WS₂, WSe₂ and VS₂ is 0.21 eV, 0.18 eV and 0.20 eV, respectively, which is consistent with the previously reported values of 0.22, 0.23 eV [61], and 0.22 eV

[42] respectively. The diffusion energy barrier of Li on 2H-MoS₂ monolayer is 0.29 eV, which is consistent with the previously reported value of 0.25 eV [18,42].

A good anode material should have a high electron and Li mobility and a large exothermic reaction energy with lithium. High electronic and ion mobility determine the rate capability and cycling performance, and a large exothermic reaction energy indicates the anode materials have a large energy storage capacity. The diffusion energy barrier is in the range between 0.17 and 0.63 eV, and most are around 0.25 eV, which indicates that all the MX₂ monolayers have a reasonable diffusion energy barrier for lithium. The metallic MX₂ monolayers and those with small bandgaps have a large adsorption energy for Li, which indicates that they are good anode materials for LIBs with high electronic and ion mobility and large energy storage capacity.

Conclusion

Using density functional theory (DFT) simulations, the stability and electronic properties of MX₂ monolayers were investigated. TiX₂, VSe₂, CrX₂, ZrX₂ and HfX₂ are energetically favourable

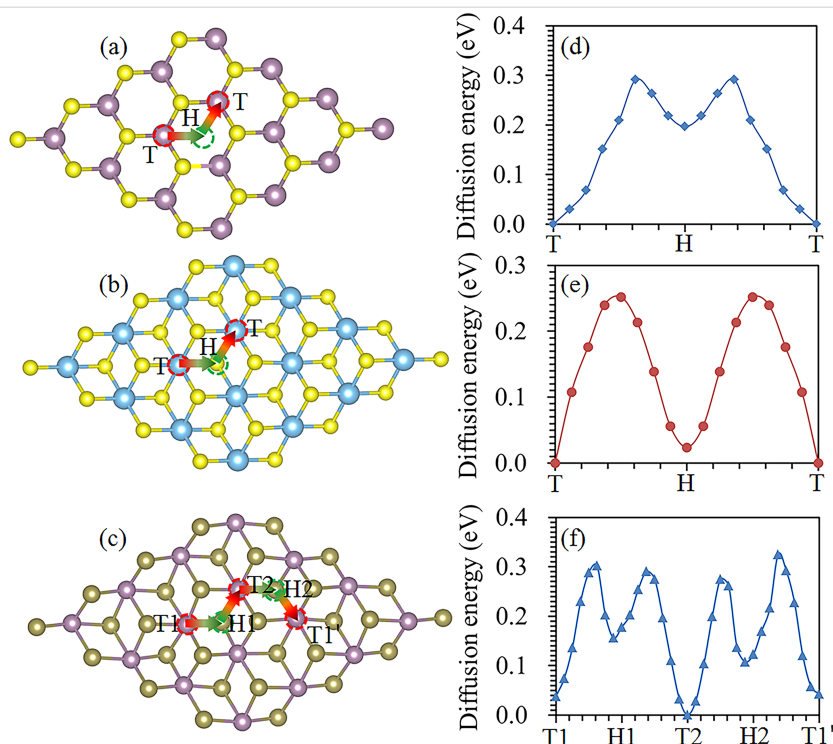


Figure 3: Possible adsorption sites and diffusion paths for Li on a monolayer of (a) 2H-, (b) 1T- and (c) 1T'-MX₂. Diffusion energy profiles for Li on (d) 2H-MoS₂, (e) 1T-TiS₂, and (f) 1T'-MoTe₂.

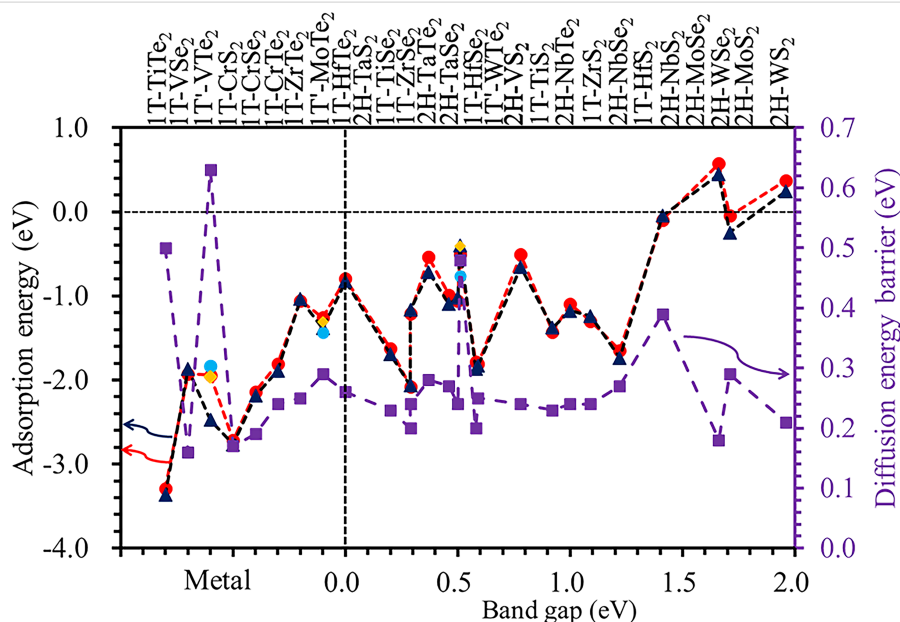


Figure 4: Adsorption energy and diffusion energy barrier for Li on MX₂ monolayers in the stable phase.

in the 1T phase, and 1T-VSe₂ can be stable both in the 2H/1T phase. The 2H phase is the stable structure for MoS₂, MoSe₂, WS₂ and WSe₂. The 1T' phase is the most energetically favourable for VTe₂, MoTe₂ and WTe₂. The 2H phase shows a semiconducting behaviour, for example, 2H-WX₂, 2H-NbX₂,

2H-TaX₂ and 2H-MoX₂. The 1T phase can be metallic or semiconducting, for example 1T-CrX₂ shows a metallic behaviour while 1T-TiX₂, 1T-ZrX₂ and 1T-HfX₂ show semiconducting and metallic behaviour with X = S/Se and X = Te, respectively. 1T'-VTe₂ and 1T'-MoTe₂ show metallic behaviour and 1T'-

WTe₂ has a narrow bandgap of 0.50 eV. The adsorption and diffusion of lithium on the stable MX₂ phase were also investigated. The results show that lithium is energetically able to adsorb on MX₂ monolayers, which are semiconductors with a narrow bandgap, and on metallic materials. Lithium cannot be adsorbed on 2H-WS₂ and 2H-WSe₂, which have a large bandgap of 1.66 and 1.96 eV, respectively. The diffusion energy barrier is in the range between 0.17 and 0.63 eV for lithium on MX₂ monolayers, and most of the materials are around 0.25 eV. It is therefore concluded that most of the MX₂ monolayers can be used as promising anode materials for lithium ion batteries.

Simulation Details

All the spin-polarized DFT calculations were performed with SIESTA code [62], in which norm-conserving pseudopotentials and a Perdew–Burke–Ernzerhof functional was used to describe the electron–ion interaction and electron exchange correlation, respectively. Numerical atomic orbits were represented as double zeta basis sets plus polarization, and a cut-off energy of 250 Ry was chosen to calculate the Hamiltonian element. The Monkhorst–Pack scheme with $11 \times 11 \times 1$ *k*-point meshes were used for integration in the irreducible Brillouin zone for the relaxation of the primitive cell. A $2 \times 2 \times 1$ *k*-point mesh was used for the calculation of adsorption and diffusion of Li on a $6 \times 6 \times 1$ supercell. As the electrochemical process involves insertion of Li ions into anode materials with a concurrent flow of electrons to compensate charge balance, and therefore, the neutral state of Li was considered in this work. The atomic positions were relaxed by using a conjugate gradient minimization until the Hellmann–Feynman force is less than 0.02 eV/Å on each atom. A vacuum spacing between the slabs and its image of greater than 20 Å is given to avoid the periodic image interactions. As the radii are different for different elements of X in MX₂ monolayers (i.e., the radius increases from S to Te in group VI), the lattice constants and bond length of the M–X bond will change for MX₂ monolayers with different X elements, which can affect the adsorption and diffusion of Li on MX₂ monolayers.

Acknowledgements

This work was financially supported by the National Natural Science Foundation of China (11474047) and the Fundamental Research Funds for the Central Universities (ZYGX2016J202). This work was carried out at National Supercomputer Center in Tianjin, and the calculations were performed on TianHe-1(A).

References

- Goodenough, J. B.; Kim, Y. *Chem. Mater.* **2010**, *22*, 587–603. doi:10.1021/cm901452z
- Cheng, C.; Zhou, G.; Du, J.; Zhang, H.; Guo, D.; Li, Q.; Wei, W.; Chen, L. *New J. Chem.* **2014**, *38*, 2250. doi:10.1039/c3nj01642k
- Chen, G.; Fu, E.; Zhou, M.; Xu, Y.; Fei, L.; Deng, S.; Chaitanya, V.; Wang, Y.; Luo, H. *J. Alloys Compd.* **2013**, *578*, 349–354. doi:10.1016/j.jallcom.2013.06.042
- Wang, L.; Dong, Z.; Wang, D.; Zhang, F.; Jin, J. *Nano Lett.* **2013**, *13*, 6244–6250. doi:10.1021/nl403715h
- Vasilyeva, E.; Nasibulin, A.; Tolochko, O.; Rudskoy, A.; Sachdev, A.; Xiao, X. Z. *Phys. Chem.* **2015**, *229*, 1429–1437. doi:10.1515/zpch-2015-0573
- Yao, Q.; Huang, C.; Yuan, Y.; Liu, Y.; Liu, S.; Deng, K.; Kan, E. *J. Phys. Chem. C* **2015**, *119*, 6923–6928. doi:10.1021/acs.jpcc.5b02130
- Kang, J.-G.; Park, J.-G.; Kim, D.-W. *Electrochem. Commun.* **2010**, *12*, 307–310. doi:10.1016/j.elecom.2009.12.025
- Wang, Z.; Su, Q.; Deng, H. *Phys. Chem. Chem. Phys.* **2013**, *15*, 8705–8709. doi:10.1039/C3CP51167G
- Radisavljevic, B.; Radenovic, A.; Brivio, J.; Giacometti, V.; Kis, A. *Nat. Nanotechnol.* **2011**, *6*, 147–150. doi:10.1038/nnano.2010.279
- Lee, C.; Yan, H.; Brus, L. E.; Heinz, T. F.; Hone, J.; Ryu, S. *ACS Nano* **2010**, *4*, 2695–2700. doi:10.1021/nn1003937
- Lauritsen, J. V.; Kibsgaard, J.; Helveg, S.; Topsøe, H.; Clausen, B. S.; Lægsgaard, E.; Besenbacher, F. *Nat. Nanotechnol.* **2007**, *2*, 53–58. doi:10.1038/nnano.2006.171
- Liu, K.-K.; Zhang, W. J.; Lee, Y.-H.; Lin, Y.-C.; Chang, M.-T.; Su, C.-Y.; Chang, C.-S.; Li, H.; Shi, Y.; Zhang, H.; Lai, C.-S.; Li, L.-J. *Nano Lett.* **2012**, *12*, 1538–1544. doi:10.1021/nl2043612
- Lee, H. S.; Min, S.-W.; Chang, Y.-G.; Park, M. K.; Nam, T.; Kim, H.; Kim, J. H.; Ryu, S.; Im, S. *Nano Lett.* **2012**, *12*, 3695–3700. doi:10.1021/nl301485q
- Lee, Y.-H.; Zhang, X.-Q.; Zhang, W.; Chang, M.-T.; Lin, C.-T.; Chang, K.-D.; Yu, Y.-C.; Wang, J. T.-W.; Chang, C.-S.; Li, L.-J.; Lin, T.-W. *Adv. Mater.* **2012**, *24*, 2320–2325. doi:10.1002/adma.201104798
- Cai, Y.; Yang, X.; Liang, T.; Dai, L.; Ma, L.; Huang, G.; Chen, W.; Chen, H.; Su, H.; Xu, M. *Nanotechnology* **2014**, *25*, 465401. doi:10.1088/0957-4484/25/46/465401
- Xiao, J.; Choi, D.; Cosimbescu, L.; Koech, P.; Liu, J.; Lemmon, J. P. *Chem. Mater.* **2010**, *22*, 4522–4524. doi:10.1021/cm101254j
- Liu, Y.; Zhao, Y.; Jiao, L.; Chen, J. J. *Mater. Chem. A* **2014**, *2*, 13109–13115. doi:10.1039/c4ta01644k
- Li, Y.; Wu, D.; Zhou, Z.; Cabrera, C. R.; Chen, Z. *J. Phys. Chem. Lett.* **2012**, *3*, 2221–2227. doi:10.1021/jz300792n
- Sun, X.; Wang, Z.; Fu, Y. Q. *Sci. Rep.* **2015**, *5*, 18712. doi:10.1038/srep18712
- Xie, X.; Chen, S.; Sun, B.; Wang, C.; Wang, G. *ChemSusChem* **2015**, *8*, 2948–2955. doi:10.1002/cssc.201500149
- Wang, X.; Li, G.; Seo, M. H.; Hassan, F. M.; Hoque, M. A.; Chen, Z. *Adv. Energy Mater.* **2015**, *5*, 1501106. doi:10.1002/aenm.201501106
- Jian, Z.; Zhao, B.; Liu, P.; Li, F.; Zheng, M.; Chen, M.; Shi, Y.; Zhou, H. *Chem. Commun.* **2014**, *50*, 1215–1217. doi:10.1039/C3CC47977C
- Hu, T.; Li, R.; Dong, J. *J. Chem. Phys.* **2013**, *139*, 174702. doi:10.1063/1.4827082
- Song, I.; Park, C.; Choi, H. C. *RSC Adv.* **2015**, *5*, 7495–7514. doi:10.1039/C4RA11852A
- Wypych, F.; Schöllhorn, R. *J. Chem. Soc., Chem. Commun.* **1992**, 1386–1388. doi:10.1039/C39920001386
- Wang, X.; Shen, X.; Wang, Z.; Yu, R.; Chen, L. *ACS Nano* **2014**, *8*, 11394–11400. doi:10.1021/nn505501v

27. Wang, L.; Xu, Z.; Wang, W.; Bai, X. *J. Am. Chem. Soc.* **2014**, *136*, 6693–6697. doi:10.1021/ja501686w
28. Cheng, Y.; Nie, A.; Zhang, Q.; Gan, L.-Y.; Shahbazian-Yassar, R.; Schwingenschlogl, U. *ACS Nano* **2014**, *8*, 11447–11453. doi:10.1021/nn505668c
29. Sun, X.; Wang, Z.; Li, Z.; Fu, Y.-Q. *Sci. Rep.* **2016**, *6*, 26666. doi:10.1038/srep26666
30. Lee, J. H.; Jang, W. S.; Han, S. W.; Baik, H. K. *Langmuir* **2014**, *30*, 9866–9873. doi:10.1021/la501349k
31. Tang, Q.; Jiang, D.-e. *ACS Catal.* **2016**, *6*, 4953–4961. doi:10.1021/acscatal.6b01211
32. Yang, E.; Ji, H.; Jung, Y. *J. Phys. Chem. C* **2015**, *119*, 26374–26380. doi:10.1021/acs.jpcc.5b09935
33. Guo, H.; Lu, N.; Wang, L.; Wu, X.; Zeng, X. C. *J. Phys. Chem. C* **2014**, *118*, 7242–7249. doi:10.1021/jp501734s
34. Tibbetts, K.; Miranda, C. R.; Meng, Y. S.; Ceder, G. *Chem. Mater.* **2007**, *19*, 5302–5308. doi:10.1021/cm0715242
35. Ambrosi, A.; Sofer, Z.; Pumera, M. *Chem. Commun.* **2015**, *51*, 8450–8453. doi:10.1039/c5cc00803d
36. Li, Y.; Duerloo, K.-A. N.; Wauson, K.; Reed, E. J. *Nat. Commun.* **2016**, *7*, 10671. doi:10.1038/ncomms10671
37. Enyashin, A. N.; Yadgarov, L.; Houben, L.; Popov, I.; Weidenbach, M.; Tenne, R.; Bar-Sadan, M.; Seifert, G. *J. Phys. Chem. C* **2011**, *115*, 24586–24591. doi:10.1021/jp2076325
38. Sun, Y.; Wang, Y.; Sun, D.; Carvalho, B. R.; Read, C. G.; Lee, C.-h.; Lin, Z.; Fujisawa, K.; Robinson, J. A.; Crespi, V. H.; Terrones, M.; Schaak, R. E. *Angew. Chem., Int. Ed.* **2016**, *55*, 2830–2834. doi:10.1002/anie.201510029
39. Duerloo, K.-A. N.; Li, Y.; Reed, E. J. *Nat. Commun.* **2014**, *5*, 4214. doi:10.1038/ncomms5214
40. Reyes-Retana, J. A.; Cervantes-Sodi, F. *Sci. Rep.* **2016**, *6*, 24093. doi:10.1038/srep24093
41. Ataca, C.; Şahin, H.; Ciraci, S. *J. Phys. Chem. C* **2012**, *116*, 8983–8999. doi:10.1021/jp212558p
42. Jing, Y.; Zhou, Z.; Cabrera, C. R.; Chen, Z. *J. Phys. Chem. C* **2013**, *117*, 25409–25413. doi:10.1021/jp410969u
43. Zhang, H.; Liu, L.-M.; Lau, W.-M. *J. Mater. Chem. A* **2013**, *1*, 10821. doi:10.1039/c3ta12098h
44. Kan, M.; Wang, B.; Lee, Y.-H.; Sun, Q. *Nano Res.* **2015**, *8*, 1348–1356. doi:10.1007/s12274-014-0626-5
45. Zhuang, H. L.; Hennig, R. G. *Phys. Rev. B* **2016**, *93*, 054429. doi:10.1103/PhysRevB.93.054429
46. Ma, Y.; Dai, Y.; Guo, M.; Niu, C.; Zhu, Y.; Huang, B. *ACS Nano* **2012**, *6*, 1695–1701. doi:10.1021/nn204667z
47. Rasmussen, F. A.; Thygesen, K. S. *J. Phys. Chem. C* **2015**, *119*, 13169–13183. doi:10.1021/acs.jpcc.5b02950
48. Ding, Y.; Wang, Y.; Ni, J.; Shi, L.; Shi, S.; Tang, W. *Physica B* **2011**, *406*, 2254–2260. doi:10.1016/j.physb.2011.03.044
49. Huang, W.; Da, H.; Liang, G. *J. Appl. Phys.* **2013**, *113*, 104304. doi:10.1063/1.4794363
50. Qian, X.; Lu, J.; Fu, L.; Li, J. *Science* **2014**, *346*, 1344–1347. doi:10.1126/science.1256815
51. Mak, K. F.; Lee, C.; Hone, J.; Shan, J.; Heinz, T. F. *Phys. Rev. Lett.* **2010**, *105*, 136805. doi:10.1103/PhysRevLett.105.136805
52. Tongay, S.; Zhou, J.; Ataca, C.; Lo, K.; Matthews, T. S.; Li, J.; Grossman, J. C.; Wu, J. *Nano Lett.* **2012**, *12*, 5576–5580. doi:10.1021/nl302584w
53. Conley, H. J.; Wang, B.; Ziegler, J. I.; Haglund, R. F., Jr.; Pantelides, S. T.; Bolotin, K. I. *Nano Lett.* **2013**, *13*, 3626–3630. doi:10.1021/nl4014748
54. Ji, Q.; Zhang, Y.; Gao, T.; Zhang, Y.; Ma, D.; Liu, M.; Chen, Y.; Qiao, X.; Tan, P.-H.; Kan, M.; Feng, J.; Sun, Q.; Liu, Z. *Nano Lett.* **2013**, *13*, 3870–3877. doi:10.1021/nl401938t
55. Huang, H. H.; Fan, X.; Singh, D. J.; Chen, H.; Jiang, Q.; Zheng, W. T. *Phys. Chem. Chem. Phys.* **2016**, *18*, 4086–4094. doi:10.1039/c5cp06706e
56. Sik Hwang, W. S.; Remskar, M.; Yan, R.; Protasenko, V.; Tahy, K.; Doo Chae, S.; Zhao, P.; Konar, A.; Xing, H.; Seabaugh, A.; Jena, D. *Appl. Phys. Lett.* **2012**, *101*, 013107. doi:10.1063/1.4732522
57. Gutiérrez, H. R.; Perea-López, N.; Elias, A. L.; Berkdemir, A.; Wang, B.; Lv, R.; López-Urías, F.; Crespi, V. H.; Terrones, H.; Terrones, M. *Nano Lett.* **2013**, *13*, 3447–3454. doi:10.1021/nl3026357
58. Kozawa, D.; Kumar, R.; Carvalho, A.; Kumar Amara, K.; Zhao, W.; Wang, S.; Toh, M.; Ribeiro, R. M.; Castro Neto, A. H.; Matsuda, K.; Eda, G. *Nat. Commun.* **2014**, *5*, 4543. doi:10.1038/ncomms5543
59. Nasr Esfahani, D.; Leenaerts, O.; Sahin, H.; Partoens, B.; Peeters, F. M. *J. Phys. Chem. C* **2015**, *119*, 10602–10609. doi:10.1021/jp510083w
60. Henkelman, G.; Jóhannesson, G.; Jónsson, H. Methods for Finding Saddle Points and Minimum Energy Path. In *Theoretical Methods in Condensed Phase Chemistry*; Schwartz, S. D., Ed.; Springer: Amsterdam, Netherlands, 2002; pp 269–302.
61. Wang, D.; Liu, L. M.; Zhao, S. J.; Hu, Z. Y.; Liu, H. *J. Phys. Chem. C* **2016**, *120*, 4779–4788. doi:10.1021/acs.jpcc.5b11677
62. Soler, J. M.; Artacho, E.; Gale, J. D.; García, A.; Junquera, J.; Ordejón, P.; Sánchez-Portal, D. *J. Phys.: Condens. Matter* **2002**, *14*, 2745–2779. doi:10.1088/0953-8984/14/11/302

License and Terms

This is an Open Access article under the terms of the Creative Commons Attribution License (<http://creativecommons.org/licenses/by/4.0>), which permits unrestricted use, distribution, and reproduction in any medium, provided the original work is properly cited.

The license is subject to the *Beilstein Journal of Nanotechnology* terms and conditions: (<http://www.beilstein-journals.org/bjnano>)

The definitive version of this article is the electronic one which can be found at:
[doi:10.3762/bjnano.8.270](https://doi.org/10.3762/bjnano.8.270)